Role of finite-size effects in the microwave and subterahertz electromagnetic response of a multiwall carbon-nanotube-based composite: Theory and interpretation of experiments

M. V. Shuba, A. V. Melnikov, A. G. Paddubskaya, P. P. Kuzhir, and S. A. Maksimenko
Institute for Nuclear Problems, Belarus State University, Bobruiskaya 11, 220050 Minsk, Belarus

C. Thomsen
Institut für Festkörperphusik, Technische Universität Berlin, Hardenbergstrasse 36, D-10623 Berlin, Germany
(Received 15 May 2013; revised manuscript received 27 June 2013; published 25 July 2013)

Electromagnetic scattering theory has been applied to calculate polarizabilities of finite-length multiwall carbon nanotubes (MWCNTs) in microwave and subterahertz ranges. The influence of the length and diameter of a MWCNT and electron relaxation time on the regime of the MWCNT interaction with an electromagnetic field has been analyzed. Significant screening effect, due to the strong depolarizing field, determines electromagnetic response of the MWCNTs field in a wide gigahertz frequency range. The main features of the gigahertz spectra of effective permittivity and electromagnetic interference shielding efficiencies of a MWCNT-based composite observed previously in experiments have been systematized and theoretically described.

DOI: 10.1103/PhysRevB.88.045436 PACS number(s): 42.70.−a, 73.25.+i, 77.84.Lf, 78.67.Ch

I. INTRODUCTION

Intensive investigation of the electromagnetic (EM) properties of carbon nanotubes (CNTs) is stimulated by the combination of unique electronic properties and the high aspect ratio (∼1000) of these nanoparticles.[1] Nowadays CNTs are considered as prospective candidates for different electromagnetic devices such as interconnects,[2–5] transmission lines,[6] and nanoantennas.[7–11]

A multiwall carbon nanotube (MWCNT) based composite material attracts great attention from researchers due to their remarkable properties of strong interaction with EM radiation at a small volume fraction of the inclusions.[12] The main efforts in the development of composite production technology are directed to increase EM interaction by means of homogenous nanotube dispersion in the dielectric matrix or by the increase of MWCNT volume fractions. However, much less attention has been paid to the possibility of EM response enhancement of MWCNT-based composite by an appropriate choice of nanotube geometrical parameters—length L and diameter D.[13,14,16]

In spite of the big progress in experimental investigations of MWCNT-based materials in the microwave regime,[13–50] the systematical theoretical analysis of the influence of EM finite size effect in MWCNTs on the effective parameters of composite material has not been comprehensively conducted. As was shown previously, the finite-length effect is very strong in the radio-frequency range,[51] whereas it can be neglected for relatively long tubes ($L > 1\ \mu$m) in the far-infrared regime.[52] In the microwave and subterahertz range the finite-length effect can be either strong or weak depending on the MWCNT parameters.[53]

Recently the scattering theory of the infinite-length MWCNT was applied to describe its response in microwave,[54] infrared,[52] and visible ranges.[52,55,56] In the present paper we apply the electromagnetic theory of scattering by the finite-length MWCNT[52] to describe systematically the parameters of individual MWCNT and MWCNT-based composite material at different regimes of nanotube interaction with microwave and subterahertz radiation. The main features in previously observed spectra of composite permittivity and shielding efficiency are well described by the proposed theory. We will demonstrate that the geometry of the MWCNTs determines the constitutive parameters of the composite materials and allows us to tune these parameters by variation of the length and diameter in particular frequency ranges. We will also show that the correct choice of the length and diameter of the MWCNTs allows us to increase significantly the interaction of the composite material with the microwave radiation without the increase of the volume fraction of the inclusions. This is extremely important for producing effective electromagnetic materials on the basis of a polymer or ceramic matrix, because only in the case of a low fraction of functional filler can one provide no degradation of their mechanical and thermal properties along with high dc conductivity and significant electromagnetic interference shielding ability.

II. THEORY

Following the theoretical electrodynamical model of a MWCNT as a finite-length multishell structure comprising of coaxial, infinitesimally thin conductive cylinders (see details in the Supplemental Material[57] and also in Ref. 52), let us consider the scattering of an electromagnetic wave by a MWCNT of length L. Let the MWCNT consist of N shells. The pth shell, $p \in [1,N]$, is of cross-sectional radius R_p, $R_N > R_{N-1} > \cdots > R_1$.

Let the cylindrical axis of the chosen MWCNT be aligned parallel to the z axis and the centroid of the MWCNT be located at the origin of the chosen cylindrical coordinate system (ρ, φ, z). As the cross-sectional radius R_N of the outermost shell is assumed to be much smaller than the free-space wavelength λ, the transverse current density in every shell is neglected. We assume that adjacent shells are incommensurate[52] and we neglect electron tunneling between shells. The axial surface conductivity of the pth shell, denoted by σ_p, is considered to be the same as the conductivity of a single-wall CNT with the

same geometrical parameters according to the formula[6,58]

$$\sigma_p = -\frac{ie^2}{\pi^2\hbar R_p(\omega + i\nu)} \sum_{s=1}^{m} \int_{1\text{st BZ}} \frac{\partial F_c}{\partial p_z} \frac{\partial \mathcal{E}_c}{\partial p_z} dp_z, \quad (1)$$

where $\hbar$ is the normalized Planck constant, e is the electron charge, and p_z is the axial projection of quasimomentum. The integer $s = 1,2,3,\ldots,m$ labels the π-electron energy bands; here m is an index appearing in the dual index (m,n) used to classify the CNTs. τ is the time of the electronic mean-free path.

The abbreviation 1st BZ restricts the variable p_z to the first Brillouin zone, and $F_c = \{1 + \exp[(\mathcal{E} - \mu_{\text{ch}})/k_B T]\}^{-1}$ is the equilibrium Fermi distribution function. Here T is the temperature, k_B is the Boltzmann constant, and μ_{ch} is the chemical potential; in graphite and undoped CNTs, $\mu_{\text{ch}} = 0$. The electron energies for zigzag and armchair shells are given respectively by

$$\mathcal{E}_c = \gamma_0 \sqrt{1 + 4\cos(ap_z)\cos\left(\frac{\pi s}{m}\right) + 4\cos^2\left(\frac{\pi s}{m}\right)} \quad (2)$$

and

$$\mathcal{E}_c = \gamma_0 \sqrt{1 + 4\cos\left(\frac{ap_z}{\sqrt{3}}\right)\cos\left(\frac{\pi s}{m}\right) + 4\cos^2\left(\frac{ap_z}{\sqrt{3}}\right)}, \quad (3)$$

where $a = 3b/2\hbar$, $b = 0.142$ nm is the interatomic distance in graphene, and $\gamma_0 \approx 2.7$ eV is the overlap integral. As we consider a frequency range below optical interband transitions the conductivity in Eq. (1) is caused only by intraband electron transitions.

Our previous investigation[53] demonstrates that MWCNTs with identical diameters and number of metallic shells have almost the same electromagnetic response in the subterahertz range. Therefore for definiteness, all calculations in the present paper shall be performed for one type of MWCNT configuration, where two consecutive semiconducting shells are followed by a metallic shell. Namely the pth shell in a MWCNT is in the $(9p + 2 - \text{mod}[p,3],0)$ configuration, where the mod$[p,3]$ function returns the remainder of p divided by 3.

For a chosen configuration the real part of the shell conductivity at room temperature versus shell diameter at different values of electron relaxation time τ is demonstrated in Fig. 1(a). One can see that small-diameter metallic shells ($2R_p < 20$ nm) have a much larger conductivity than semiconducting shells of the same diameter. As for thick shells ($2R_p > 20$ nm), the conductivity of both semiconducting and metallic shells are close to each other.[2] The shell conductivity increases with increasing diameter due to the contribution from the intraband transition in bands with a small gap energy $E_g < k_B T$. An analogical situation occurs in small-gap quasimetallic single-wall carbon nanotubes: Their conductivity at room temperature is close to the conductivity of metallic nanotubes.[59]

As can be seen from Fig. 1(a) the real part of the shell conductivity increases proportionally to the relaxation time. Thus relaxation time is a very important parameter that determines the mechanism of MWCNT interaction with subterahertz radiation. As MWCNTs produced in practice have an imperfect structure with a lot of defects in the crystal lattice, we shall take for our calculation the value of relaxation time varied from 5 to 20 fs.

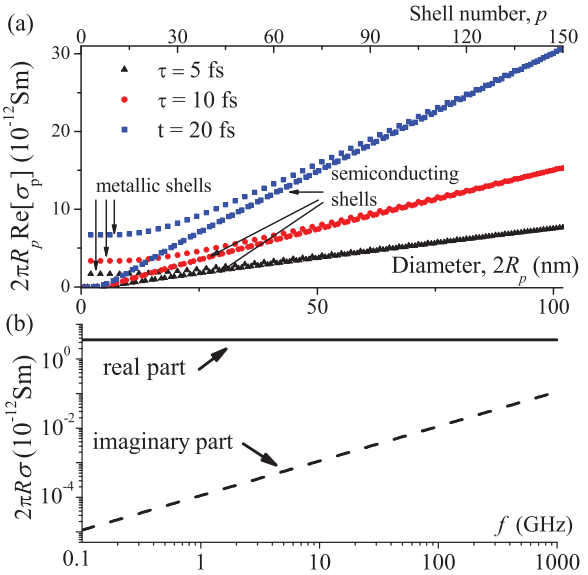

FIG. 1. (Color online) (a) The real part of the pth-shell conductance versus the shell number (or shell diameter) at frequency $f = 10$ GHz and temperature 300 K. (b) The frequency dependence of the real and imaginary part of the conductivity of shell with chiral indexes (673,0) and diameter 52.7 nm, $\tau = 5$ fs.

Figure 1(b) shows the subterahertz spectra of the real and imaginary parts of the conductivity of the big-radius semiconducting shell. In the subterahertz range, due to the small value of electron relaxation time $\tau \ll 1/\omega$, the relations $\text{Re}[\sigma] \gg \text{Im}[\sigma]$ and $\text{Re}[\sigma(\omega)] \simeq$ const are true for the surface conductivity σ of both metallic and semiconducting shells. Such relations indicate the strong attenuation of the eigenwaves in a hypothetic infinite-length MWCNT[52] and consequently their small real part of the polarizability and large absorption per unit length. However, in realistic composite materials the finite-length effect in MWCNTs can influence strongly the electromagnetic parameters of the composite media (see Sec. III).

Figure 2 shows the frequency dependence of MWCNT polarizability α at different diameters D and lengths L. The imaginary part of α has a peak in the subterahertz range at a frequency which we define as f_p. The value f_p increases with increasing MWCNT diameter D [Fig. 2(d)] or decreasing MWCNT length L [Fig. 2(c)], and divides the spectra into two different regimes of MWCNT interaction with incident radiation: quasistatic regime and dynamical regime.

A. Quasistatic regime

In the range $f \ll f_p$ $\text{Re}[\alpha]|_{f \ll f_p} \approx \text{Re}[\alpha]|_{f \to 0}$, that corresponds to the quasistatic regime, the real part of the MWCNT polarizability is the same as in the electrostatic case at $f \to 0$. The polarizability is influenced strongly by the finite-length effects leading to strong screening effects.[51] The surface current density on the outermost shells induces an axial depolarizing field, which is approximately equal to and oppositely directed to the axial component of the incident field. Therefore, the axial component of the total field on the surface

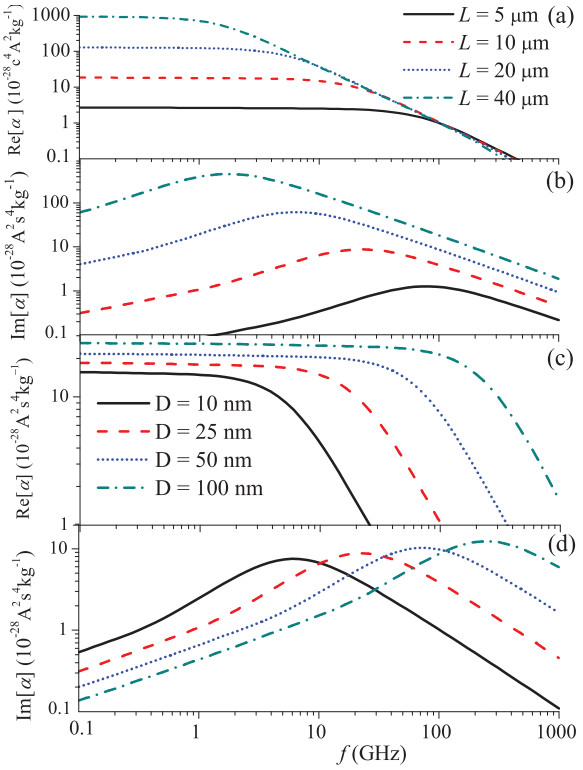

FIG. 2. (Color online) The frequency dependence of the real and imaginary part of the MWCNT polarizability at different tube lengths L [(a) and (b)] and diameters D [(c) and (d)]. $D = 25$ nm [(a) and (b)], $L = 10$ μm [(c) and (d)], and $\tau = 5$ fs.

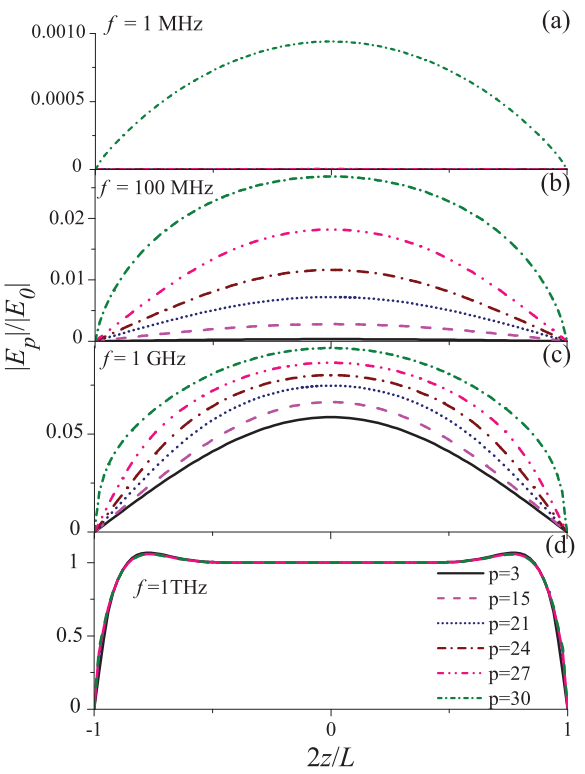

FIG. 3. (Color online) The axial total field distribution on the surface of the pth shell at frequency (a) 1 MHz, (b) 100 MHz, (c) 1 GHz, and (d) 1 THz for a MWCNT of diameter 20 nm and length 10 μm, $\tau = 5$ fs. The incident electric field E_0 is aligned parallel to the z axis.

of any internal shell is smaller than the axial component of the incident field. In other words, the outermost shells of a finite-length MWCNT screen the internal shells.

Figure 3 demonstrates the total field distribution on the surface of pth shells for a MWCNT of length 20 μm at different frequencies of incident field. At a frequency of 1 MHz the screening effect is very strong—the total field in the outmost shell is much larger than in the internal shells but much smaller than the incident field [Fig. 3(a)]. At higher frequencies the screening effect is weaker—at 100 MHz the total field is significant on the surface of the several outmost external shells [Fig. 3(b)].

Let $q \in [0, N-1]$ be the largest number for which $E_N/E_{N-q} \geqslant e$ is true, where $e = 2.71825\ldots, E_N$ and E_{N-q} are the amplitude of the total axial field on the surface of the outmost shell and the $N-q$th shell, respectively. Then the number $N_{\text{ext}} = 1 + q$ is analogous to the penetration depth: The larger the value of N_{ext}, the more the penetration.

Figure 4 shows the dependence of N_{ext} on the values of f, L, and τ for a 30-shell MWCNT exposed to a plane wave with an electric field parallel to the tube axis. Clearly the screening effect is stronger for smaller frequencies [Figs. 4(a) and 4(b)], shorter MWNTs [Figs. 4(a) and 4(d)], and larger electron relaxation time [Figs. 4(c) and 4(e)]. For thin MWCNTs ($D < 20$ nm) the value of N_{ext} practically does not depend on the diameter D, however for thick MWCNTs ($D > 20$ nm) the value of N_{ext} decreases with increasing nanotube diameter [see Fig. 4(b)]. That is explained by the increase of shell conductivity with increasing shell diameter [Fig. 1(a)].

As was noted in Ref. 53 in the quasistatic regime, the finite-length MWCNT can be considered as interconnect, where the outer N_{ext} shells can be exploited for shielding the remaining inner shells from external spurious radiation, while the inner metallic shells can be used to propagate signals. Due to the stronger screening effect for thicker tubes, they have a smaller imaginary part of polarizability (smaller energy dissipation) in the quasielectrostatic regime than the thinner MWCNTs [see Fig. 2(d) at $f < 6$ GHz]. However, the real part of the polarizability is larger for thick MWCNTs than for thin MWCNTs of the same length [see Fig. 2(a) at $f < 6$ GHz].

The polarizability of the long MWCNT is larger than for the short MWCNT in the quasistatic regime [see Figs. 2(a) and 2(b)] due to the following reasons.

(i) In the case of the short MWCNT exposed by an external field, the separated surface charges of opposite sign on the nanotube edges are close to each other and create a strong depolarizing field. This field suppresses current on the nanotube surface resulting in a small nanotube polarizability. The increase of the nanotube length is accompanied by the increase of the distance between separated charges and consequently by the decrease of the depolarizing field.

(ii) The polarizability of the MWCNT is calculated as an integral over the current along the tube, so that the polarizability should increase with increasing nanotube length even in the case of a negligibly small depolarizing field. This

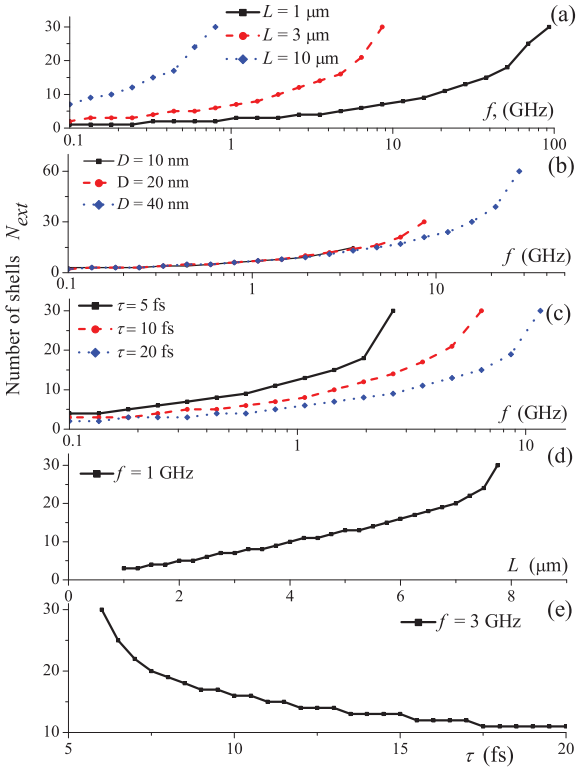

FIG. 4. (Color online) Frequency dependence of N_{ext} for MWCNTs of (a) different lengths L, (b) diameters D ($L = 3$ μm), and (c) electron relaxation times τ ($L = 5$ μm). The value of N_{ext} versus the (d) MWCNT length at $f = 1$ GHz and (e) electron relaxation time at $f = 3$ GHz ($L = 5$ μm). The MWCNT has a diameter of 20 nm (30 shells) and $\tau = 5$ fs. The incident electric field is aligned parallel to the tube axis.

explains the strong dependence of the nanotube polarizability on the nanotube length.

B. Dynamical regime

In the frequency range of $f \geqslant f_p$—dynamical regime—the values Re[α] and Im[α] decrease with increasing frequency (Fig. 2). In the dynamical regime the screening effect in the MWCNT becomes less significant,[54] i.e., electromagnetic fields penetrate deeper inside the MWCNT [compare Figs. 3(b) and 3(c)], resulting in an increase of the electromagnetic absorption cross section of these particles.

At frequencies $f \gg f_p$ the total axial field on the MWCNT shells is practically equal to the incident field [Fig. 3(d)], so that the surface current density $J(z)$ on the surface of the pth shell of the MWCNT exposed to the external electric field E_0 obeys with high accuracy the Ohms law

$$J_p(z) = \sigma_p E_0(z), \tag{4}$$

which is indeed the first Born approximation of scattering theory. Note that the surface current (4) does not satisfy the edge conditions $J_p(L/2) = 0$ for the finite-length MWCNT. However, the error is strongly localized in the vicinity of the edges [see Fig. 3(d)] and therefore does not influence the field formation in the far-field region. In such an approximation the polarizability of the MWCNT is proportional to its length.

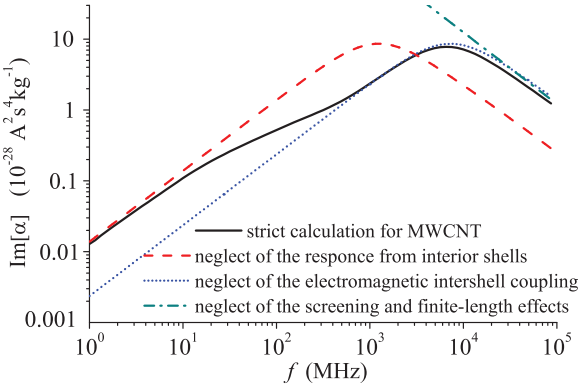

FIG. 5. (Color online) Frequency dependence of a MWCNT of length $L = 10$ μm and diameter $D = 10$ nm, and $\tau = 5$ fs calculated on the basis of different models: The self-consistent model of finite-length coaxial cylinder[52] (solid line); the non-self-consistent model of coaxial cylinder based on Eq. (4) (dash-dotted line) omitting finite-length and screening effects; the model of single-wall tube with diameter 10 nm and effective conductance equaled to the conductance of outmost metallic shell of the MWCNT (dashed line); or a sum of conductance of all the shells in the MWCNT (dotted line).

In order to illustrate the influence of finite length and screening effects on the electromagnetic response of the MWCNT, in Fig. 5 we calculated the imaginary part of the polarizability of the MWCNT using different approximations. The solid line in Fig. 5 gives the polarizability of the calculated MWCNT taking into account both finite-length and screening effects. The dash-dotted line in Fig. 5 presents calculation of Im[α], which omits screening and finite-length effects, supposing the effective field in the shells to be equal to the incident field [Eq. (4)]. To point out the contribution from the outmost metallic shell in the quasistatic regime we calculate the value of Im[α] for the MWCNT when the conductivity of all shells except the outmost metallic shell is equal to zero (dashed line in Fig. 5). And finally, the dotted line in Fig. 5 demonstrates the polarizability of a single-wall tube with the diameter equal to that of the MWCNTs and the effective conductance equal to the sum of the conductances of all the shells in the MWCNTs; this calculation does not take into account electromagnetic coupling of the shells in the MWCNTs.

As shown in Fig. 5 the quasistatic regime for the MWCNT of length 10 μm and diameter 10 nm is realized at frequencies $f < 10$ MHz and can be well described by the model of a single-wall cylinder. In the dynamical regime $f > 10$ GHz the finite-length effect and screening effect disappear and the frequency dependence of the MWCNT polarizability has Druder behavior. The electromagnetic coupling between the shells can be neglected in the range of $f > 1$ GHz. The intermediate regime (10 MHz $< f <$ 1 GHz) is characterized by the partial penetration of the axial field inside the MWCNT and cannot be calculated on the basis of simple models.

III. EFFECTIVE PERMITTIVITY OF A MWCNT-BASED COMPOSITE

Let us consider a dilute composite material comprising of randomly dispersed, randomly oriented, MWCNTs. In order to

illustrate the influence of length and diameter of the MWCNTs on the effective parameter of composite material we apply the Waterman-Truell formula[60,61] adopted to estimate the relative permittivity of a MWCNT-based composite material:

$$\varepsilon_{\text{eff}} = \varepsilon_h + \frac{1}{3\varepsilon_0}\sum_j \int\int_0^\infty \alpha_j(L,D)N_j(L,D)dLdD, \quad (5)$$

where ε_h is relative permittivity of the host media; $\varepsilon_0 = 8.85 \times 10^{-12}$ F/m; the factor 1/3 in Eq. (5) is due to the random orientations of the MWCNTs; and the distribution function $N_j(L,D)$ describes the number density of the MWCNTs of type j with length L and diameter D. $\alpha_j(L,D)$ is the axial polarizability of the MWCNT inclusion of type j, which enumerate MWCNTs with different configurations of metallic and semiconducting shells inside the MWCNTs. To illustrate the influence of the finite size effect on the value ε_{eff} in our calculation we shall take only one configuration, where two consecutive semiconducting shells are followed by a metallic shell (see previous section). Furthermore, in our calculations we shall take the following parameters: $\varepsilon_h = 2.2$; n (MWCNT volume fraction occupied by the MWCNTs, each conceived as a cylinder of volume $\pi D^2 L/4$) shall be taken to be equal 0.02; and the electron relaxation time $\tau = 5$ fs has been used under calculations of the axial shell conductivity of MWCNTs. Formula (5) does not take into account local field effects that occur at high volume fraction of the inclusions.

Figure 6 demonstrates the frequency dependence of the effective relative permittivity of a MWCNT-based composite at different nanotube lengths and the same CNT volume fraction. These spectra demonstrate a strong dependence of the effective permittivity on MWCNT length. In the low frequency range ($f < 10$ GHz) the real and imaginary parts of the effective permittivity are larger for a composite comprising of longer tubes. However at higher frequencies the value of Re[ϵ_{eff}] can be larger for a composite comprising of short-length tubes [compare the lines for $L = 40$ μm and $L = 10$ μm at $f > 8$ GHz in Fig. 6(a)]. The value of Im[ϵ_{eff}] has a maximum at frequency f_p, which depends on the nanotube length. The permittivity spectra in Fig. 6 can be divided into three different regimes corresponding to different interactions of incident radiation with MWCNTs.

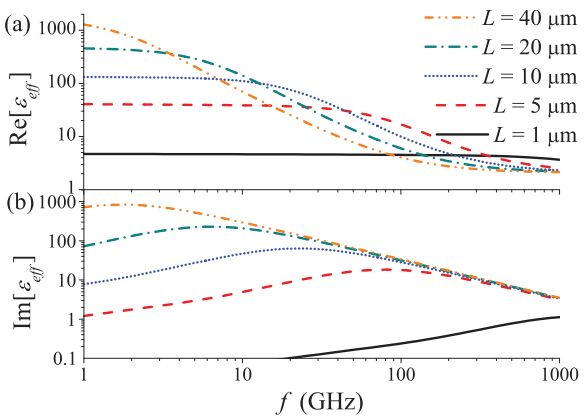

FIG. 6. (Color online) The spectra of (a) real and (b) imaginary parts of effective relative permittivity of the composite comprising of MWCNTs of different lengths L. The MWCNT diameter is 25 nm.

(1) *Quasistatic regime* ($f \ll f_p$). The value Im[ϵ_{eff}] increases and value Re[ϵ_{eff}] decreases as frequency increases, and the loss tangent $\delta \equiv$ Im[ϵ_{eff}]/Re[ϵ_{eff}] $\ll 1$. In this regime the strong screening effect prevents the effective interaction of the MWCNTs with electromagnetic radiation, as only the outmost shell contributes into the MWCNT response. The composite parameters in the quasistatic regime have been measured in Refs. 17,19,23, and 32.

(2) *Dynamical regime* ($f > f_p$). Both values Im[ϵ_{eff}] and Re[ϵ_{eff}] simultaneously decrease with increasing frequency and $\delta > 1$; such a regime was observed for composites in Refs. 21,30,31,34,45,49, and 50.

It does not matter in the dynamical regime if either the MWCNTs form or do not form a conductive network. As the screening effect is absent, the field penetrates fully inside the MWCNT and the absorption of the composite is maximal. In order to achieve the dynamical regime for all MWCNTs in the composite and consequently to achieve maximal possible absorption of the MWCNT-based composite, the length of the MWCNTs should be more than the minimal length, presented in Table I for different nanotube diameters D and frequency ranges. As is shown in Table I the thicker tubes should be longer to provide the penetration of the electromagnetic field up to the innermost shell and provide the maximal absorption of electromagnetic energy by every shell.

Partially dynamical regimes can occur for short MWCNTs if they form a conductive network in the dielectric matrix. The electrical contact between adjacent MWCNTs in the network leads to electron tunneling between the tubes and to partial suppression of finite-length and screening effects. As a result the effective length of the touched tubes can exceed the realistic length and the dynamical regime partially realized for a short-length MWCNT composite.

(3) *Intermediate regime* ($f \approx f_p$). The value Re[ϵ_{eff}] decreases with increasing frequency and is comparable with Im[ϵ_{eff}], i.e., $\delta \approx 1$.[29,34,39,48]

It is often obtained for MWCNT-based composites at low volume fraction in the gigahertz frequency range that $\delta < 1$ and both values Re[ϵ_{eff}] and Im[ϵ_{eff}] decrease with increasing frequency.[18,20,22,24–29,31,34] Such a regime is absent in Fig. 6.

In order to explain such composite parameters one should take into account the nanotube length distribution in the composite. For simplicity we calculated the effective permittivity of the composite comprising of long-length MWCNTs [Fig. 7(a)] short-length MWCNTs [Fig. 7(b)], and a mixture of short- and long-length MWCNTs [Fig. 7(c)]. As Fig. 7(c) shows at a frequency range from 3 to 20 GHz $\delta < 1$, both

TABLE I. Minimal MWCNT length (in micrometers) that corresponds to the dynamical regime when the finite-length and consequently the screening effects can be neglected. D is the MWCNT diameter.

Frequency range	$D = 5$ nm	$D = 10$ nm	$D = 25$ nm	$D = 50$ nm
$f > 1$ GHz	25	40	80	150
$f > 10$ GHz	7.5	11	23	43
$f > 100$ GHz	2.2	3	6.5	12
$f > 1$ THz	0.6	0.9	1.8	3.4

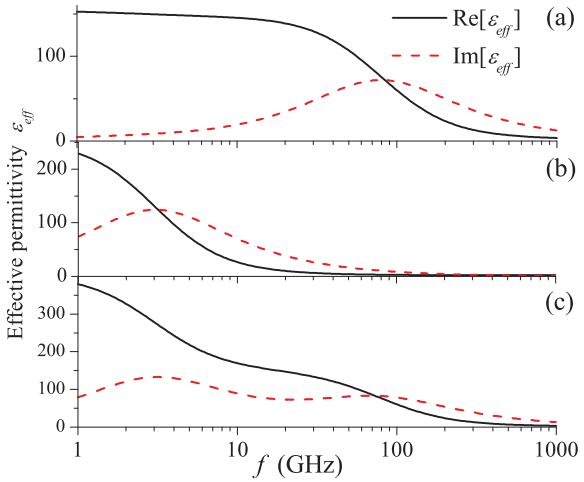

FIG. 7. (Color online) The spectra of effective relative permittivity of composite material comprising of (a) short MWCNTs of length $L_1 = 5$ μm at volume fraction $n_1 = 7.5\%$; (b) long MWCNTs of length $L_2 = 30$ μm at volume fraction $n_2 = 0.5\%$; and (c) a mixture of short and long MWCNTs with volume fraction $n_1 = 7.5\%$ and $n_2 = 0.5\%$, respectively. The MWCNT diameter is 25 nm.

values Re[ϵ_{eff}] and Im[ϵ_{eff}] decrease as frequency increases; in such a range the short-length tubes are in the quasistatic regime and contribute predominantly to the value of Re[ϵ_{eff}], whereas long-length tubes are in the dynamical regime and contribute to the value of Im[ϵ_{eff}]. So the dielectric parameters of the composite comprising of a mixture of different length tubes can be different from the parameters of a composite comprising of identical nanotubes [compare Figs. 7(a) and 7(b) with Fig. 7(c)]. Thus, the dielectric permittivity of the MWCNT composite can be tuned by means of variation of the MWCNT length distribution function.

Figure 8 demonstrates the frequency dependence of the effective permittivity of the MWCNT composite for different nanotube diameters at the same nanotube length and volume fraction. As shown in Fig. 8 both values Im[ϵ_{eff}] and Re[ϵ_{eff}] are larger for thinner MWCNTs at frequencies $f < 30$ GHz. Though the real part of the polarizability of thinner MWCNTs is smaller [see Fig. 2(c)], their number density is larger than

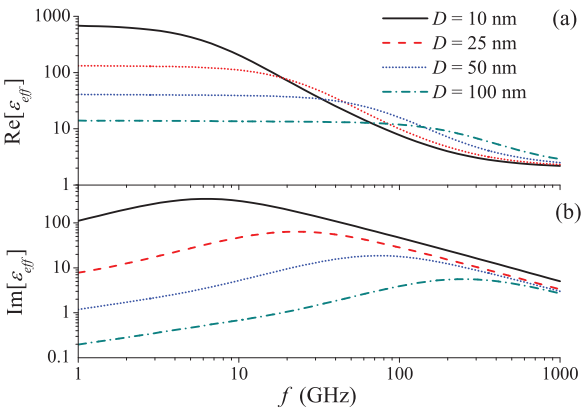

FIG. 8. (Color online) Spectra of the (a) real and (b) imaginary parts of effective relative permittivity of a composite comprising of MWCNTs of different diameters D and identical length 10 μm.

the number density of thicker MWCNTs at the same volume fraction. This explains the larger value of Re[ϵ_{eff}] for a composite comprising of thinner tubes. The peak frequency f_p in the spectra of Im[$\epsilon_{\text{eff}}(\omega)$] is smaller for thinner MWCNTs. As a result the value of Re[ϵ_{eff}] can be larger for thicker nanotubes (see Fig. 8 at $f > 30$ GHz). Thus, both MWCNT length and diameter are very important parameters that determine effective parameters of a MWCNT-based composite.

IV. SHIELDING EFFICIENCY OF A MWCNT-BASED COMPOSITE

Using the Fresnel formulas we have calculated the transmittance T, reflectance, and absorbance of the composite plate. Figure 9 demonstrates the spectra of electromagnetic interference shielding effectiveness (SE $= -10\log_{10}$ T) of the composite comprising of MWCNTs of different lengths and diameters at the same volume fraction. As shown in Fig. 9 the SE is larger for longer and thinner MWCNTs; this was experimentally demonstrated for a MWCNT composite of different nanotube diameters[14,38] and lengths.[13] Let us also note that according to Fig. 8 SE increases as frequency increases, that has been observed in Refs. 21,31,32,40–43, and 45–47.

However, as was reported in Refs. 13, 19, 25, 31, and 33–38 the value SE can remain practically constant or decrease as frequency increases in narrow frequency ranges that are realized at small SE (<15 dB), when interference phenomena in composite slab occur. As was noted in Ref. 33 at a low volume fraction the reflection losses dominate over the dissipation losses in the composite and determine SE decreases with increasing frequency. Figure 10 demonstrates the electromagnetic interference shielding efficiency SE(T) and the contribution from reflection SE(R) and dissipation SE(A) losses for the MWCNT composite at a different volume fraction. The oscillations in the spectra of SE(T), SE(R), and SE(A) are due to the interference effect in the composite layer. As shown in Fig. 10 at low (high) frequency the reflection (dissipation) losses prevail. There is a narrow frequency range where reflection losses prevail and SE(T) decreases with increasing

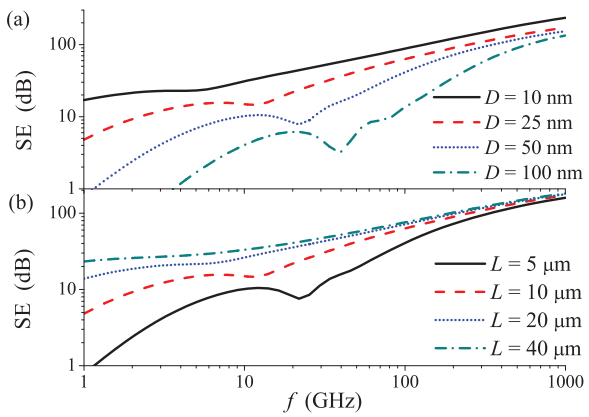

FIG. 9. (Color online) The spectra of electromagnetic interference shielding effectiveness SE of a MWCNT-based composite plate with a thickness of 1 mm at different nanotube (a) diameters D and (b) lengths L. Nanotube volume fraction $n = 0.02$. A composite comprises of identical MWCNTs with (a) lengths 10 μm and (b) diameters 25 nm.

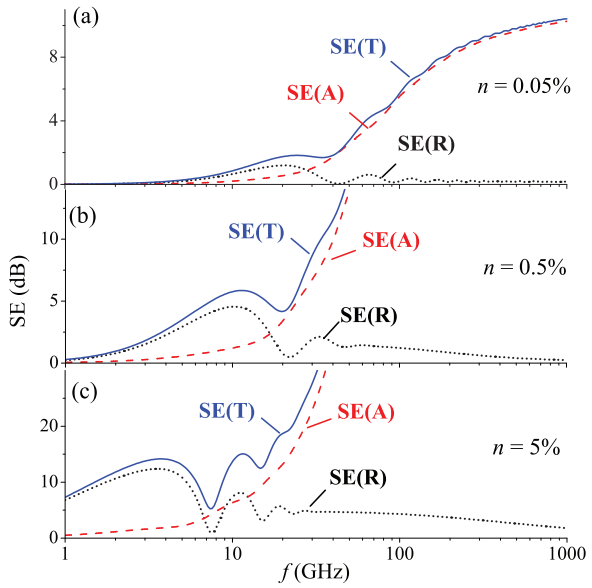

FIG. 10. (Color online) Frequency dependence of total shielding efficiency SE(T) of a MWCNT-based composite with a thickness of 2 mm at different nanotube volume fractions: (a) $n = 0.05\%$, (b) $n = 0.5\%$, and (c) $n = 5\%$. The contribution into SE(T) from reflection SE(R) and absorption SE(A) are also presented by dotted and dashed lines, respectively. A composite comprises of identical MWCNTs with length 5 μm and diameter 25 nm.

frequency, this range shifts to low frequency with increasing nanotube volume fraction [compare Figs. 10(a)–10(c)].

V. CONCLUSION

The scattering theory was applied to calculate the polarizability of an individual MWCNT as an electrically small finite-length coaxial cylinder. The influence of the nanotube length and diameter on the spectra of the MWCNT polarizability has been illustrated. The interaction of the MWCNT with EM radiation in the quasistatical and dynamical regimes has been analyzed in microwave and subterahertz ranges. In the quasistatic regime the strong depolarizing field in the finite-length MWCNT leads to the screening effect—weak penetration of the axial field component inside the MWCNTs. The comprehensive study of the screening effect in thick finite-length MWCNTs in the quasistatic regime is presented. The dependence of the field penetration depth on the nanotube length, diameter, electron relaxation time, and radiation frequency has been demonstrated.

The relation between macroscopic parameters of the MWCNT-based composite and microscopic parameters of the inclusions (length, diameter) has been established. The main features of the gigahertz spectra of the effective parameters of the MWCNTs composite, previously observed in experiments, have been systematized and theoretically described. We have shown that big variety of the experimental data on the electromagnetic parameters of the MWCNT-based composites can be divided into four groups corresponding to the different regimes of the MWCNT interaction with radiation.

We have demonstrated that one of the possible ways to increase interaction of the composite with electromagnetic radiation is the appropriate choice of the geometrical parameters of the MWCNTs. Presented analysis gives a theoretical upper limit of effective permittivity and shielding efficiency of a MWCNT-based composite that can be achieved in practice at a given nanotube length and diameter. As a rule, effective permittivity and shielding efficiency obtained in experiments are about 5–10 times less than predicted by theory. There are several obstacles such as nanotube agglomeration and cutting during the preparation process that hinder the production of composite material with a highly effective electromagnetic response and low volume fraction of MWCNTs as inclusions. We hope that the conducted theoretical analysis stimulates the technological progress in realization of MWCNT-based composite material with improved electromagnetic parameters in microwave and subterahertz ranges.

ACKNOWLEDGMENT

This research was partially supported by BRFFR (Belarus) under Projects F12R-030 and F12MV-004; and EU FP7 under Projects FP7-318617 FAEMCAR, FP7-247007 CACOMEL, and FP7-266529 BY-NanoERA.

[1] S. Reich, C. Thomsen, and J. Maultzsch, *Carbon Nanotubes. Basic Concepts and Physical Properties* (Wiley-VCH, Berlin, 2004).
[2] A. Naeemi and J. D. Meindl, IEEE Electron Device Lett. **27**, 338 (2006).
[3] H. Li and K. Banerjee, IEEE Trans. Electron Devices **56**, 2202 (2009).
[4] S. Bellucci and P. Onorato, J. Appl. Phys. **108**, 073704 (2010).
[5] A. Maffucci, G. Miano, and F. Villone, IEEE Trans. Adv. Pack. **31**, 692 (2008).
[6] G. Ya. Slepyan, S. A. Maksimenko, A. Lakhtakia, O. Yevtushenko, and A. V. Gusakov, Phys. Rev. B **60**, 17136 (1999).
[7] G. W. Hanson, IEEE Trans. Antennas Propag. **53**, 3426 (2005).
[8] P. J. Burke, S. Li, and Z. Yu, IEEE Trans. Nanotechnol. **5**, 314 (2006).
[9] G. Ya. Slepyan, M. V. Shuba, S. A. Maksimenko, and A. Lakhtakia, Phys. Rev. B **73**, 195416 (2006).
[10] M. V. Shuba, S. A. Maksimenko, and G. Ya. Slepyan, J. Comput. Theor. Nanosci. **6**, 2016 (2009).
[11] M. V. Shuba, A. G. Paddubskaya, A. O. Plyushch, P. P. Kuzhir, G. Ya. Slepyan, S. A. Maksimenko, V. K. Ksenevich, P. Buka, D. Seliuta, I. Kasalynas, J. Macutkevic, G. Valusis, C. Thomsen, and A. Lakhtakia, Phys. Rev. B **85**, 165435 (2012).
[12] F. Qin and C. Brosseau, J. Appl. Phys. **111**, 061301 (2012).
[13] L.-L. Wang, B.-K. Tay, K.-Y. See, Z. Sun, L.-K. Tan, and D. Lu, Carbon **47**, 1905 (2009).
[14] I. N. Mazov, V. L. Kuznetsov, S. I. Moseenkov, A. V. Ishchenko, A. I. Romanenko, O. B. Anikeeva, T. I. Buryakov, E. Yu. Korovin, V. A. Zhuravlev, and V. I. Suslyaev, Fullerenes, Nanotubes Carbon Nanostruct. **18**, 505 (2010).

[15]V. I. Suslyaev, V. L. Kuznetsov, V. A. Zhuravlev, I. N. Mazov, E. Yu. Korovin, S. I. Moseenkov, and K. V. Dorozhkin, Russ. Phys. J. **55**, 970 (2012).
[16]P. P. Kuzhir, A. G. Paddubskaya, M. V. Shuba, S. A. Maksimenko, A. Celzard, V. Fierro, G. Amaral-Labat, A. Pizzi, G. Valusis, J. Macutkevic, M. Ivanov, J. Banys, S. Bistarelli, and A. Cataldo, J. Nanophoton. **6**, 061715 (2012).
[17]P. C. P. Watts, D. R. Ponnampalam, W. K. Hsu, A. Barnes, and B. Chambers, Chem. Phys. Lett. **378**, 609 (2003).
[18]C. P. W. Paul, W. K. Hsu, A. Barnes, and B. Chambers, Adv. Mater. **15**, 600 (2003).
[19]J. S. Im, J. G. Kim, S.-H. Lee, and Y.-S. Lee, Colloids Surf. A **364**, 151 (2010).
[20]J. S. Im, I. J. Park, S. J. In, T. Kim, and Y.-S. Lee, J. Fluorine Chem. **130**, 1111 (2009).
[21]C. Xiang, Y. Pan, and J. Guo, Ceram. Int. **33**, 1293 (2007).
[22]T. Xiao, H. L. Yang, and G. P. Zhang, J. Appl. Phys. **110**, 024902 (2011).
[23]S. H. Park, P. Thielemann, P. Asbeck, and P. R. Bandaru, Appl. Phys. Lett. **94**, 243111 (2009).
[24]R. K. Srivastava, T. N. Narayanan, A. P. R. Mary, M. R. Anantharaman, A. Srivastava, R. Vajtai, and P. M. Ajayan, Appl. Phys. Lett. **99**, 113116 (2011).
[25]Z. Liu, G. Bai, Y. Huang, Y. Ma, F. Du, F. Li, T. Guo, and Y. Chen, Carbon **45**, 821 (2007).
[26]S. Pfeifer, S-H. Park, and P. R. Bandaru, ECS Solid State Lett. **2**, M5 (2013).
[27]D. S. Bychanok, M. A. Kanygin, A. V. Okotrub, M. V. Shuba, A. G. Paddubskaya, A. O. Pliushch, P. P. Kuzhir, and S. A. Maksimenko, JETP Lett. **93**, 607 (2011).
[28]A. Mdarhri, F. Carmona, C. Brosseau, and P. Delhaes, J. Appl. Phys. **103**, 054303 (2008).
[29]A. C. Xiang, Y. Pan, X. Liu, X. Sun, X. Shi, and J. Guo, Appl. Phys. Lett. **87**, 123103 (2005).
[30]C. A. Grimes, E. C. Dickey, C. Mungle, K. G. Ong, and D. Qian, J. Appl. Phys. **90**, 4134 (2001).
[31]Y. Huang, N. Li, Y. Ma, F. Du, F. Li, X. He, X. Lin, H. Gao, and Y. Chen, Carbon **45**, 1614 (2007).
[32]A. Saib, L. Bednarz, R. Daussin, C. Bailly, X. Lou, J.-M. Thomassin, C. Pagnoulle, C. Detrembleur, R. Jerome, and I. Huynen, IEEE Trans. Microwave Theory Tech. **54**, 2745 (2006).
[33]S.-H. Park, P. T. Theilmann, P. M. Asbeck, and P. R. Bandaru, IEEE Trans. Nanotech. **9**, 464 (2010).
[34]A. Fletcher, M. C. Gupta, K. L. Dudley, and E. Vedeler, Comput. Sci. Technol. **70**, 953 (2010).
[35]Y. Yang, M. C. Gupta, K. L. Dudley, and R. W. Lawrence, Nano Lett. **5**, 2131 (2005).
[36]H. M. Kim, K. Kim, S. J. Lee, J. Joo, H. S. Yoon, S. J. Cho, S. C. Lyu, and C. J. Lee, Curr. Appl. Phys. **4**, 577 (2004).
[37]H. M. Kim, K. Kim, C. Y. Lee, J. Joo, S. J. Cho, H. S. Yoon, D. A. Pejakovic, J. W. Yoo, and A. J. Epstein, Appl. Phys. Lett. **84**, 589 (2004).
[38]L. Vovchenko, L. Matzui, V. Oliynyk, V. Launetz, and A. Lazarenko, Mol. Cryst. Liq. Cryst. **497**, 46 (2008).
[39]Y. Li, C. Chen, J.-T. Li, S. Zhang, Y. Ni, S. Cai, and J. Huang, Nanoscale Res. Lett. **5**, 1170 (2010).
[40]Y. Li, C. Chen, S. Zhang, Y. Ni, and J. Huang, Appl. Surf. Sci. **254**, 5766 (2008).
[41]J.-M. Thomassin, I. Huynen, R. Jerome, and Ch. Detrembleur, Polymer **51**, 115 (2010).
[42]C. K. Jang, J. H. Park, and J. Y. Jaung, Mater. Res. Bull. **47**, 2767 (2012).
[43]C.-S. Zhang, Q.-Q. Ni, S.-Y. Fu, and K. Kurashiki, Comp. Sci. Technol. **67**, 2973 (2007).
[44]M. Arjmand, T. Apperley, M. Okoniewski, and U. Sundararaj, Carbon **50**, 5126 (2012).
[45]J.-M. Thomassin, C. Pagnoulle, L. Bednarz, I. Huynen, R. Jeromeaand, and C. Detrembleura, J. Mat. Chem. **18**, 792 (2008).
[46]C-C. M. Ma, Y.-L. Huang, H.-C. Kuan, and Y.-S. Chiu, J. Polymer Sci B: Polymer Phys. **43**, 345 (2005).
[47]N. C. Das and S. Maiti, J. Mater. Sci. **43**, 1920 (2008).
[48]G. XuChun, W. KunLin, W. JinQuan, L. RuiTao, S. QinKe, J. Yi, W. Chen, Z. HongWei, and W. DeHai, Sci. China Ser. E: Tech. Sci. **52**, 227 (2009).
[49]M. Imai, K. Akiyama, T. Tanaka, and E. Sano, Comp. Sci. Technol. **70**, 1564 (2010).
[50]R. C. Che, L. M. Peng, X. F. Duan, Q. Chen, and X. L. Liang, Adv. Mater. **16**, 401 (2004).
[51]M. V. Shuba, G. Ya. Slepyan, S. A. Maksimenko, and G. W. Hanson, J. Appl. Phys. **108**, 114302 (2010).
[52]M. V. Shuba, G. Ya. Slepyan, S. A. Maksimenko, C. Thomsen, and A. Lakhtakia, Phys. Rev. B **79**, 155403 (2009).
[53]S. A. Maksimenko, G. Ya. Slepyan, M. V. Shuba, and A. Lakhtakia, *IEEE Electrical Design of Advanced Packaging and Systems (EDAPS) Symposium, Hangzhou, China* (IEEE, Piscataway, NJ, 2011), p. 1.
[54]J. A. Berres and G. W. Hanson, IEEE Trans. Antennas Propag. **59**, 3098 (2011).
[55]S. M. Mikki and A. A. Kishk, Prog. Electromag. Res. B **17**, 49 (2009).
[56]H. Khosravi and A. Moradi, Opt. Commun. **284**, 2629 (2011).
[57]See Supplemental Material at http://link.aps.org/supplemental/10.1103/PhysRevB.88.045436 for the theory of electromagnetic wave scattering by a finite length MWCNT.
[58]S. A. Maksimenko and G. Ya. Slepyan, in *Electromagnetic Fields in Unconventional Materials and Structures*, edited by O. N. Singh and A. Lakhtakia (Wiley, New York, 2000), pp. 217–255.
[59]G. Ya. Slepyan, M. V. Shuba, S. A. Maksimenko, C. Thomsen, and A. Lakhtakia, Phys. Rev. B **81**, 205423 (2010).
[60]P. C. Waterman and R. Truell, J. Math. Phys. **2**, 512 (1961).
[61]A. Lakhtakia, Int. J. Electron. **75**, 1243 (1993).